Adjustable Bolted Steel Plate Connection: Measured Behavior of Bolts

during Field Installation and Numerical Parametric Investigation

Evan J. Gerbo, S.M.ASCE¹; Ashley P. Thrall, A.M.ASCE²; Theodore P. Zoli, P.E., M.ASCE³

4 ABSTRACT

- This paper presents an experimental investigation of bolt behavior in adjustable bolted steel plate connections during field installation and a numerical finite element (FE) parametric investigation of the impact of (1) bolt diameter, (2) plate thickness, and (3) member flange thickness on the strains induced in the plates and bolts during field installation. The adjustable connection consists of prefabricated cold bent plates which are further bent during field installation (via bolt tightening) to form moment-resisting joints between steel members. The connection is adjustable, as the bolt tightening field installation process changes the connection angle in-situ to accommo-11 date additional angles or manufacturing and erection tolerances. This paper presents the residual bolt surface strains, measured using the full-field photographic technique Digital Image Correla-13 tion, providing unprecedented information on the behavior of high-strength bolts. An FE modeling approach for predicting strains in the plates and bolts is developed and validated against measured 15 data. Parametric studies are then performed using the validated FE models with varying bolt diam-16 eter, plate thickness, and member flange thickness. Research results are relevant to any misaligned 17 (i.e., non-flush) bolted connections, offering insight into strains from force fitting.
- ¹⁹ Author Keywords: Bolted steel connection; Cold bending; Prefabrication; Rapid Erection;

20 INTRODUCTION

An adjustable bolted steel plate connection [Figure 1, Gerbo et al. (2018)] is a new approach

¹PhD Candidate, Kinetic Structures Laboratory, Department of Civil & Environmental Engineering & Earth Sciences, University of Notre Dame, Notre Dame, IN 46556. E-mail: egerbo@nd.edu

²Myron and Rosemary Noble Associate Professor of Structural Engineering, Kinetic Structures Laboratory, Department of Civil & Environmental Engineering & Earth Sciences, University of Notre Dame, Notre Dame, IN 46556. (corresponding author) E-mail: athrall@nd.edu

³National Bridge Chief Engineer, HNTB Corp., Empire State Building, 350 5th Ave., 57th Floor, New York, NY 10118. E-mail: tzoli@hntb.com

for the rapid erection of steel buildings and bridges. The slip-critical splice connection consists of prefabricated cold bent plates (prebent via a press brake), constituting a kit-of-parts. The plates are further bent in the field via bolt tightening until an adaptation of the turn-of-nut criteria are met [i.e., after plies are brought into firm contact with one another, additional turns are performed consistent with those recommended by the turn-of-nut criteria (Research Council on Structural 26 Connections, 2014)] to join flanges of angled wide flange members. Flanges (member, hereafter) 27 are connected by three of these bent splice plates (plates, hereafter): a top plate and two narrower 28 bottom plates straddling the web (Figure 1C). Webs are connected by straight splices in dou-29 ble shear. By connecting the flanges and webs independently, a moment-resisting connection is 30 achieved. The connection is adjustable, as the bolt tightening field installation process enables the kit-of-parts of bent plates to join a variety of angles or accommodate manufacturing and erection tolerances.

The authors have previously (1) experimentally and numerically investigated the surface strains 34 induced in the plates due to prefabrication (Gerbo et al., 2016) and (2) experimentally investigated the plate surface strains due to field installation (Gerbo et al., 2018). This prior investigation found that (1) differences in connection ply angles at or below 2.5° keep plate field installation strains within reasonable bounds (0.01 mm/mm), (2) a criss-cross bolt tightening pattern with one turn of each bolt per increment was preferred for evenly distributed plate strains, and (3) the maximum field installation strain induced in the plates is primarily dependent on differences in connection ply angles (Gerbo et al., 2018). This prior research has focused only on the behavior of the plates. There is no existing research on the behavior of the bolts in the adjustable bolted steel plate con-42 nection, specifically, or for the more general case of misaligned (i.e., non-flush plies) bolted splice connections. While there is a great deal of research on bolted steel connections (e.g., Kulak et al. 2001, Douty and McGuire 1965, Munse et al. 1959, Rajasekharan et al. 1974, Chesson and Munse 1965, AASHTO 2014), this existing research considers the connection plies to have no more than 1/20.0 (2.86°) relative slope between plies at the initiation of tightening. This research investigates connections with greater relative slopes between plies [i.e., up to $1/7.60 (7.50^{\circ})$]. While the focus is on the adjustable bolted steel plate connection, the results are relevant for misaligned bolted splice connections, generally. Misaligned bolted splice connections often occur during construction and are handled by force fitting. The effects of this force fitting are not well understood or controlled. During bolt tightening, of either the adjustable bolted steel plate connection or misaligned connections, the high-strength bolts are subjected to bending as they plastically deform the plies of the connection into firm contact with each other, in addition to the axial pre-tension typical of slip-critical connections. It is critical to investigate both the bending and axial strains induced in the bolts during field installation to ultimately understand the impact of installation on the connection's behavior.

58 OBJECTIVES AND SCOPE

The objectives of this paper are to (1) experimentally investigate strains induced in bolts of 59 adjustable bolted steel plate connections during field installation and (2) numerically investigate 60 the impact of bolt diameter, plate thickness, and member flange thickness on the plate and bolt 61 strains induced during field installation. The full-field, residual surface strains of bolts in 14 experimentally tested scenarios (Table 1) are measured using three-dimensional (3D) digital image correlation (DIC) to investigate the effect of the bolt-tightening procedure, amount and direction of bending, and plate angle. A finite element (FE) numerical modeling approach for the field installation process is developed and validated by comparing these measured residual bolt strains with FE predictions. The measured plate strains presented in Gerbo et al. (2018) are also compared with FE predictions. A parametric study, using the validated FE modeling approach, is then performed to investigate the effect of bolt diameter, plate thickness, and member flange thickness on the residual bolt strains due to field installation and plate strains induced during field installation and the cumulative fabrication process (including also strains from prefabrication via press brake). This research provides unprecedented information on the behavior of high-strength bolts and the results are relevant to any misaligned (i.e., non-flush) bolted connections.

74 EXPERIMENTAL PROGRAM

75

A total of 14 scenarios were experimentally tested to investigate the effect of (1) bolt-tightening

procedure, (2) amount and direction of plate bending during field installation, and (3) plate angle on the field installation strains induced in the bolts [Table 1, Figure 1E and 1F, Gerbo et al. (2018)]. The geometric parameters of the tested connection (Figure 2A and 2B) were selected in Gerbo 78 et al. (2018) for greatest versatility with respect to manufacturing or erection tolerances and member dimensions. The kit-of-parts of bent plates is intentionally comprised of as few a number of 80 unique parts as possible. The angle of the top plates (γ) is chosen to be equal to that of the bottom 81 plates (β) , with values of 5° , 10° , and 15° as well as a non-bent 0° option. Similarly, the radius of curvature of the top plate (r_t) is equal to that of the bottom plate (r_b) , with a magnitude of 102 mm 83 (4 in.). The length of the top plate (l_1) is the same as the bottom plate (l_2) . These plates will join 84 members at varying angles (α), with a difference in ply angles, $\delta = \alpha - \gamma$. 85

The field installation was tested by connecting the top flanges of ASTM A992 (ASTM, 2015) 86 W10x88 wide flange sections with 3 ASTM A36 (ASTM, 2014b) plates: 1 top plate and 2 bottom 87 plates. Note that the ends of the W10x88 wide flange sections were not mitered in the experimental program for simplicity, but would be in practice as envisioned in Figure 1A - 1C. The thickness of the plates (t_s) were chosen to be approximately half the thickness of the member flange (t_m) , typical of bolted splice connections in double shear. 165 mm (6.5 in.) long ASTM A325 (ASTM, 91 2014a) bolts with 19.1 mm (0.750 in.) diameter (d_b) were used in all tested scenarios. Two, 31.8 mm (1.25 in.) long hardened stainless steel spacers were used to facilitate experimental testing, as well as 5 ASTM F436 (ASTM, 2018) washers (1 washer was placed between the plates and each spacer, as well as another washer between the bolt head and spacer, and 2 washers were placed between the nut and spacer). Plate hole diameters (d_{ph}) were oversized bolt holes $[d_{ph} = 23.8 \text{ mm}]$ (0.9375 in.)] with end distances (l_3) set to 76.2 mm (3.00 in.) and member hole diameters (d_{mh}) were long-slotted holes [d_{mh} = 47.6 mm (1.875 in.)] based on geometric studies performed in Gerbo et al. (2018). An additional control scenario using flush plies (i.e., plies are flat and parallel, with only two plates and one bolt) was also tested (Scenario 14). 100

The test procedure involved first loosely assembling the plates and bolt assemblies on the reaction frame (Figure 1E) and adjusting the bolt assemblies to have the same nut position [within

0.508 mm (0.0200 in.)]. A controlled tightening procedure, using the torque wrench and tools shown in Figure 1F, was then performed until the plies of the connection were in full contact. The 104 bolt was held in position during tightening of the nut in specified increments (Table 1) until con-105 tact is achieved at each bolting location [contact was determined by attempting to fit a 0.254 mm 106 (0.0100 in.) shim between the plate and member]. After contact was achieved at all bolting loca-107 tions, a final 1 turn of each bolt was completed to satisfy the adaptation of the turn-of-nut criteria 108 (Research Council on Structural Connections, 2014). Match marks were made on the bolt head 109 and nut in the initial untightened position. These marks were then used to track the total number 110 of turns at each nut throughout tightening. 111

Residual strains of the bolts were measured using DIC. DIC is a noncontact photographic 112 technique that uses photogrammetric triangulation and pattern recognition to calculate full-field 113 surface strains. To facilitate pattern recognition, a random pattern was etched onto the shank of 114 the bolts using CerMark LMM-6000 Metal Laser Marking Spray (Ferro, 2016) and a laser cutter 115 (Universal Laser Cutter, VLS 6.60, 50W laser). The DIC photographs were taken with 6 separate 116 readings per bolt prior to testing and after testing (i.e., after connection disassembly) to calculate 117 the residual strains from field installation. The data was assembled to form 3D surface strain 118 maps that were unwrapped to form a flat image (e.g., Figure 3, positive indicates tension and negative indicates compression throughout the paper). The unwrapping used a series of fitted polar coordinate systems, along the bolt length, to minimize distortion in the final unwrapped image. The coordinate system origin is at the side of the bolt facing away from the connection centerline, at mid-height of the bolt (Figure 3). To quantify noise, several DIC measurements were taken prior 123 to testing when the bolts were under no load. The standard deviation of these measurements yields 124 noise levels on the order of 0.00052 mm/mm. This represents 0.8% of the peak strains observed in 125 this study (approximately 0.06 mm/mm). There was loss of DIC data in locations that experience 126 surface abrasion, which generally align with locations of compression. 127

Gerbo et al. (2018) reported the surface plate strains from these tests, also measured using DIC.

Throughout the paper, the discussed plate strains are those at full tightening. Reported bolt strains

are residual strains (i.e., measured after the connection has been disassembled).

131 NUMERICAL MODELING

132

133

134

135

136

137

3D FE models of field installation were built in ABAQUS Standard (ABAQUS, 2014). Nonlinear material properties were modeled using an isotropic hardening model based on measured true stress-strain relationships for the plate [A36, ASTM (2014b)] and bolt [A325, ASTM (2014a)] steels [see Gerbo et al. (2018)]. Nonlinear geometry was considered. C3D8R elements were used, with a typical mesh size of 1.59 mm (0.0625 in.) in the plates, 3.17 mm (0.125 in.) in the member, and 1.27 mm (0.0500 in.) in the bolts.

The models use symmetry along two planes to limit computational expense. To enforce sym-138 metry, translation restraints in the z direction are applied to the member and plate surfaces cut by 139 the xy plane, and translation restraints in the x direction are applied to the plate surfaces cut by 140 the yz plane (Figure 4A). Only a portion of the member is modeled: half of the web and 305 mm 141 (12.0 in.) of the member length. Boundary conditions provide restraint against all translation at 142 the cut faces of the member to simulate a rigid reaction frame (Figure 4B). Stability in the vertical 143 (y) direction is maintained through the contact interactions between the member and plates, and 144 between the plates and bolt assembly. The bolt assembly has no boundary conditions, with stabil-145 ity derived from contact interactions. Tangential behavior of the contact interactions is modeled 146 with a penalty friction formulation (with the exception of the bolt shank to nut interaction which 147 is considered frictionless as part of a simplification related to thread interaction), and assumed to 148 have frictional coefficients of 0.33, as recommended for steel on steel faying surfaces (Kulak et al. 2001 and AASHTO 2014). The normal behavior of the contact interactions is modeled with a linear stiffness formulation [spring constant of 27.1 GPa/mm (100,000 ksi/in)] to allow for convergence. To aid convergence, fillets with radius 1.27 mm (0.0500 in) are used at all corners involved 152 in contact definitions. 153

Prefabrication is first modeled, using the validated approach developed in Gerbo et al. (2016), to provide an initial strain state in the plates which is imported into the field installation model.

This ensures that the steel hardness in the prebent region of the plates is properly simulated.

Bolt tightening is achieved through a prescribed relative displacement between the inside of the nut and the tip of the bolt (Figure 4A and 4B), modeling the displacement achieved in the experimental procedure. After completion of tightening, the bolt is released from its interactions to simulate the disassembly process. For comparison with the measured data, the predicted FE plate strains are those at full tightening. Predicted bolts strains are residual strains after disassembly.

The thread interaction between the nut and bolt is not modeled, but a reduced cross-section based on measurements of the bolt (28.5% reduction) is used in the threaded region for all reported bolt data. For the models predicting the plate strains, a constant cross-section cylindrical bolt was used due to numerical issues in predicting plate strains near the plate-bolt contact.

In the FE models of the experimentally tested scenarios, extra washers and spacers (which facilitated testing) were used to replicate the physical assembly. This hardware was simplified in the parametric models to include only a single washer at the bolt head to plate contact, and a single washer at the nut to plate contact, resulting in shorter bolts required to reach through the connection hardware. The bolt lengths in the parametric models vary based on the grip length [i.e., twice the plate thickness (t_s) plus the member thickness (t_m)].

BEHAVIOR OF BOLTS AND PLATES DURING FIELD INSTALLATION

During field installation, the bolts are placed in axial tension by tightening. This tension is resisted by bending in the plates until contact with the member. After contact, additional bolt tension applies a clamping force between the plies of the member and plates, providing resistance to slip under loading. As the plies are non-flush, combined tension and bending occurs during bolt tightening due to the eccentric contact at the bolt head and nut, causing bending in the bolts. Additional bending results from contact with the plate holes. The resulting strain pattern is a combination of tension and bending [e.g., Figure 3, where bending in Scenario 1 is indicated with regions of concentrated tension (blue) and compression (red) along the bolt shank]. Figure 5 shows the amount and location of bolt bending in Scenario 1 by plotting the curvature (ϕ) as a function of longitudinal coordinate of the bolt. Curvature is calculated by fitting planes to the longitudinal bolt surface strains (ϵ_y) , which are divided into regions perpendicular to the bolt axis creating many

section cuts. The slope of the fitted planes, relative to the longitudinal (z) axis, is the curvature. A moving average is then used to smooth out noise from this plane fitting process. The location of the 185 curvature for Scenario 1, i.e., along the bolt shank as opposed to the reduced regions, indicates that 186 bolt bending is primarily due to contact with the plates. In contrast, a flush slip-critical connection 187 (Scenario 14) featured measured and predicted strains that were only axial (data not shown for 188 conciseness). 189

Effect of Bolt Tightening Procedure 190

192

197

199

200

201

203

204

205

206

207

208

209

Due to the relatively large number of turns required to close the adjustable connection (varying 191 from 3 to 12 turns), compared to a conventional connection with initially flush plies, it is desirable to minimize the time required to install the connection. One means of reducing construction time is to increase the number of bolt turns completed in each increment. When using single turn increments in a criss-cross pattern (Scenario 1), the measured longitudinal surface bolt strains are predominantly symmetric among the four bolts (Figure 3). Small differences are observed in the 196 lower bending region [i.e., y = -40.0 mm (1.57 in.), where bolts 1 and 2 (Figure 1D) experience tensile strains up to 0.0447 mm/mm, bolt 3 experiences 0.0483 mm/mm and bolt 4 experiences just 198 0.0411 mm/mm]. This localized asymmetry is likely caused by the tightening procedure which proceeded from bolt 1 to bolt 4 for Scenario 1. Figure 5 shows similar locations and magnitudes of curvature for Scenario 1 among the four bolts (with peak curvature magnitudes ranging from 0.113 deg/mm to 0.186 deg/mm, a difference of less than 40 percent). 202

By increasing the number of turns per tightening increment to 3 (Scenario 2), the measured longitudinal surface strains in bolts 3 and 4 are higher than bolts 1 and 2 (with bolts 3 and 4 reaching strain magnitudes of 0.0710 mm/mm and bolts 1 and 2 reaching 0.0657 mm/mm). The measured curvature in bolts 3 and 4 (with peak magnitudes of 0.290 deg/mm) is also much higher than bolts 1 and 2 (with peak magnitudes of 0.141 deg/mm), as well as higher than all bolts of Scenario 1 (Figure 5). The lower strains and curvature in the first two bolts are due to rigid body movement of the plates during the first turns which reduces the bolt deformation. The increased strains and curvature in bolts 3 and 4 are due to the additional restraint imposed by the tightening of the first two bolts, therefore increasing the required bolt deformation at contact with the plates for the last two bolts. Increasing the increment further, such that each bolt is tightened to contact before moving onto the next bolt (Scenario 3) resulted in fracturing bolt 3. This combined tension and torsion failure caused a fracture in the threaded region of the 165 mm (6.5 in.) long A325 bolts that closed the 50.5 mm (1.99 in.) total thickness of plies. Therefore, to achieve relatively uniform strains and curvature among the bolts, the recommended procedure is 1 turn of each bolt per increment. This is consistent with the recommendations in Gerbo et al. (2018) to maintain symmetric strains in the plates.

219

220

221

222

223

224

225

226

227

The tightening pattern (criss-cross, clockwise, or counter-clockwise), while maintaining 1 turn per increment, was investigated by comparing bolt strains in Scenarios 1, 4, and 5. All three scenarios resulted in similar distributions and magnitudes of strains in the bolts (full-field data for Scenarios 4 and 5 not shown for conciseness). The curvature in all bolts for both Scenario 4 and 5 are similar to one another and similar to Scenario 1 (Figure 5). It was found in Gerbo et al. (2018) that circular tightening procedures (i.e., Scenarios 4 and 5) lead to diagonal strain banding in the plates. Therefore it is recommended to use a criss-cross tightening pattern for field installation. All scenarios discussed throughout the rest of the paper use the recommended tightening procedure of 1 turn per increment in a criss-cross pattern.

The FE models feature only one bolt (due to symmetry) and assume a uniform, simultaneous 228 bolt tightening procedure. The FE predictions accurately capture the peak measured bolt strains (with peak predicted longitudinal strains of 0.0510 mm/mm and peak measured longitudinal strains 230 ranging from approximately 0.0310 mm/mm to 0.0514 mm/mm) and curvatures (with peak pre-231 dicted curvature of 0.202 deg/mm and peak measured curvatures ranging from 0.113 deg/mm to 232 0.186 deg/mm) with the recommended tightening procedure of 1 turn per increment in a crisscross pattern (Scenario 1). The differences between the FE predictions and the measured results in 234 Scenario 2 (with measured peak curvatures ranging from 0.103 deg/mm to 0.305 deg/mm) can be 235 attributed to the asymmetric behavior that occurs with this tightening increment which could not 236 be captured by a symmetric FE model.

Effect of Varying Amount and Direction of Plate Bend

Varying the amount of plate bending (i.e., the magnitude of δ) and the direction of plate bending (i.e., the sign of δ , where positive indicates further bending and negative indicates bending back toward flat) affects bolt behavior during field installation. During plate bending, bolts are subjected to bending from eccentric bolt head and nut contact and from plate contact on the shank of the bolt. An indicator of bolt bending is the amount of bolt deformation (e_b , Figure 2C, Table 1) which can be approximated as:

$$e_b = e_h - (d_{vh} - d_b) \tag{1}$$

where e_h is the eccentricity between the plate holes, calculated as:

$$e_h = e_o + \frac{e_d}{\cos \alpha} \tag{2}$$

where e_o is the eccentricity due to the vertical offset of the plates relative to the member angle and e_d is the effect of the deformed shape on horizontal component of the plate lengths (Figure 2C-E). Assuming the deformed shapes of the top and bottom plates have identical profiles in elevation and are axially rigid, e_o is calculated as follows:

$$e_o = |(t_m + t_s) \tan \alpha| \tag{3}$$

To account for the difference in deformed profiles of the top and bottom plates, an approximation can be made that the plates are composed of two rigid bodies connected by a plastic hinge. If δ is positive, the plastic hinge in the top plate will occur at the member contact location and the plastic hinge in the bottom plate will occur at the net section. If δ is negative, the opposite is true. The change in the horizontal components of the plate lengths due to this simplified deformed shape (e_d) is calculated as follows:

$$e_d = \begin{cases} l_4(\cos \gamma - \cos \alpha) & \text{if } \delta \ge 0\\ g(\cos \gamma - \cos \alpha) & \text{if } \delta \le 0 \end{cases}$$

$$(4)$$

where l_4 is the distance from the edge of the member to the center of the member hole and g is the gap between the members at the top flange (Figure 2). Note that these approximations assume the 257 holes are smaller in the plates (i.e., oversized holes) than in the member (i.e., long slots). 258

259

260

261

262

263

264

265

266

267

268

269

270

271

272

274

277

High values of bolt deformation, e_b , correspond to higher longitudinal strains and curvature in the bolts, as shown for example in Scenario 1 ($\delta = 7.5^{\circ}$, Figures 3 and 6). By decreasing the amount of bending and therefore reducing e_b , the magnitude of curvature in Scenario 6 ($\delta = 2.5^{\circ}$) is reduced (Figure 6). The distribution of curvature along the bolt length remains the same, with concentrations along the bolt shank at contact locations with the plates demonstrating plate contact as the primary contributor to bending.

When the direction of plate bending is reversed in Scenario 8 ($\delta = -7.5^{\circ}$), the bolt deformation, e_b is reduced as the plates are bent back toward flat and are no longer in contact with the bolt. The measured full-field strains show almost no strain in the bolt shank and reduced data loss (compared to Scenario 1) from gouging which indicates limited plate contact. The FE predictions indicate that strains are concentrated in the reduced cross-section representing the threaded region. Increased curvature is also predicted in the reduced cross-section (Figure 6). The location of this curvature in the reduced cross-section indicates that bending is primarily due to eccentric contact of the bolt head and nut. A reduced magnitude of plate bending in Scenario 7 ($\delta = -2.5^{\circ}$) results in similar strain and curvature distributions (Figure 6), with lower magnitudes.

Figure 7 shows the relationships between e_b and curvature for the experimentally tested scenarios. Here the curvature is calculated separately for the bolt shank compared to the reduced 275 cross-section. Note that the curvature values are from the FE models as these are better able to 276 capture curvature in the threaded region of the bolts (modeled as a reduced cross-section). High values of e_b [i.e., $e_b > 3.18$ mm (0.125 in.)] indicate bending predominantly in the bolt shank due to plate contact. The reduced cross-section is sufficiently far from the shear plane (as spacers to 279

facilitate the experimental program move the threaded region beyond the shear plane) to not be affected by this bending. However, there is some bending indicated by the small peak curvature in the reduced cross-section. Conversely, small value and negative values of e_b [i.e., $e_b < 3.18$ mm (0.125 in.)] feature peak curvature in the reduced cross-section as bending is dominated by eccentric bolt head and nut contact.

Effect of Varying Plate Angle

These trends relating the bolt deformation (e_b) to the bending in the bolts are also observed for varying plate angles $(\gamma = \beta)$, considering bending of $\delta = \pm 2.5^{\circ}$.

In scenarios with low initial plate angles (i.e., $\gamma = \beta \le 10^{\circ}$, Scenarios 9, 10, and 11), the induced strains are concentrated in the reduced cross-section (data not shown for conciseness). Consistent with prior findings for scenarios with low e_b , the curvature is predominantly in the reduced cross-section region, indicating bending from eccentric bolt head and nut contact (Figure 7 and 8).

Scenarios with high initial plate angles (i.e., $\gamma = \beta \ge 10^{\circ}$, Scenarios 12 and 13) show similar trends with e_b . Scenario 13, with a high value of e_b , exhibits high curvature in the bolt shank region, indicating bending due to plate contact (Figure 7 and 8). Scenario 12, with a much lower value of e_b , shows almost no bending.

The numerical predictions for Scenario 13 indicate a higher magnitude of curvature at the top 297 bending location [0.215 deg/mm (5.46 deg/in.) peak curvature at y = 8.01 mm (0.315 in.)] than 298 the bottom bending location [0.0100 deg/mm (0.254 deg/in.) at y = -39.6 mm (1.56 in.)]. This 299 is in contrast to the measured data which indicates more symmetric curvature at both of the plate 300 contact locations. The FE models for this type of scenario (i.e., positive δ) show that the bending 301 in the bolts occurs first at the top plate contact location followed by bending at the bottom plate 302 contact location at the last part of tightening. Bending at the top plate location occurs first because 303 the bolt force is higher nearer the tightening location as compared to the bottom plate location 304 where frictional losses reduce the force in the bolt. The FE model for Scenario 13 shows that 305 while the plates and members are in contact (per the experimental protocol) and an additional turn-

of-nut was also performed, the spacer by the head of the bolt does not come into firm contact with the washer. The DIC photographs of this scenario confirm this condition, but to a lesser degree. 308 Additional FE modeling indicated that if the bolt were tightened an additional turn, bending would 309 have occurred also at the bottom plate contact location, and the spacers would come into firm 310 contact with the washers. This demonstrates that more strict tightening criteria, which requires 311 firm contact between the bolt head, washer, and plates, are needed. This will be investigated in 312 future research focusing on the connection strength. Scenario 13 was particularly susceptible to 313 this effect because it features the highest plate angle ($\gamma = \beta = 15^{\circ}$) and bends to the highest member 314 angle ($\alpha = 17.5^{\circ}$). 315

Summary 316

323

325

The field bending process induces residual strains in the bolts in both axial and bending domi-317 nant patterns. The magnitude of bending is related to the bolt deformation (e_b) which also indicates if the bending is from plate contact in the bolt shank region [$e_b > 3.18$ mm (0.125 in.)] or from eccentric bolt head and nut contact resulting in bending in the threaded region [$e_b < 3.18$ mm 320 (0.125 in.)321

Overall, the FE predictions agree closely with the measured results, both in the distribution and 322 magnitude of longitudinal bolt strains. Through these comparisons, the FE modeling approach can be considered validated with respect to the bolt strains induced during field installation. 324

NUMERICAL PREDICTIONS OF PLATE STRAINS

To validate the numerical modeling approach with respect to the plate behavior, FE predictions 326 for circumferential plate surface strains (ϵ_x , i.e., strain in the x direction in Figure 9) were compared 327 with measured results. The measured strain induced during field installation [reported in Gerbo 328 et al. (2018)], as well as the measured cumulative strains from prefabrication [reported in Gerbo 329 et al. (2016)] and field installation (cumulative fabrication process, hereafter) are compared to the 330 FE predictions. 331

2 Benchmark Comparison

350

351

352

353

354

355

356

357

The measured and predicted full-field circumferential strains of a benchmark case [Scenario 333 6, selected because it is between the minimum and maximum considered member angles (α) , and 334 follows the $|\delta| \le 2.5^{\circ}$ recommendation of Gerbo et al. (2018)] show close agreement in magnitude 335 and distribution (Figure 10), for both the field bending and cumulative fabrication process. FE 336 predictions of the field bending process indicate peak circumferential surface strains of 0.00467 337 mm/mm in the top plates and -0.00291 mm/mm in the bottom plates. The predicted field bending 338 strains in the bottom plate are spread out smoothly over the center region [approximately 50-100] 339 mm (2-4 in.) width] of the plate, whereas the predicted field bending strains in the top plate are concentrated more locally [approximately 20-30 mm (0.8-1.2 in.) width], directly over the contact locations with the member. Circumferential surface strain data is also plotted along longitudinal Lines A-D (Figure 9) on the plate surfaces (Figure 11). Generally, the measured and predicted data agree closely. However, the measured peak field bending strains in the top plate are higher in magnitude (reaching 0.0102 mm/mm) than the predicted results (0.00467 mm/mm) along Lines 345 B and C at x = 90 mm (3.54 in.). This can be attributed to a combination of asymmetry in the 346 reaction frame and the bolt tightening process (Gerbo et al., 2018). The FE model is unable to cap-347 ture these effects because it assumes symmetry across two planes and therefore assumes uniform 348 simultaneous bolt tightening and a perfect reaction frame. 349

The cumulative strain patterns are dominated by the prefabrication process (Figure 10 and 11). The peak predicted and measured cumulative strains in Scenario 6 occurs in the prebent region of the top plate. The small predicted strain concentrations along Lines B and C at x = 90 mm (3.54 in.) due to contact with the member during field bending are an order of magnitude lower than strains induced during prefabrication and are insignificant in comparison to the cumulative strains (approximate peak strains of 0.06 mm/mm). The cumulative strains in the bottom plates are even less affected by the field bending process, representing almost solely the prefabrication process.

Overall, the measured results agree well with the FE predictions.

Varying Amount and Direction of Plate Bend

Figure 11 demonstrates that the FE modeling approach is valid for varying amounts and direction of bending. The field bending strains are affected by the prefabrication process as the cold bending via press brake induces an initial strain state in the center region, locally hardening the steel. This alters the distribution of field bending strains when field bending strains coincide with prefabrication strains in environments of positive δ (Gerbo et al., 2018). For example, the peak field bending strains are pushed to the edge of the prebent region in the bottom plates of Scenario 1 (see Lines A and D in Figure 11). This is also present in Scenario 6, but is less clearly observed as field bending strains are lower due to the smaller δ . This demonstrates the importance of including the initial strain state in the FE models.

There are a few locations where the measured results and FE predictions for field bending strains differ. The measured strains are approximately double the predicted FE strains in Scenario 8 along Line A and D in the prebent region of the bottom plates. This is because Scenario 8 induces significant bending in the direction opposite that of fabrication. The Bauschinger effect lowers the yield stress due to this reversal of plastic strain in the prebent portion of the plates. The FE material model used an isotropic hardening model that does not incorporate the Bauschinger effect, and thus predicts lower strain magnitudes from field bending than the measured DIC results for Scenario 8 in the prebent region. This could be improved by the use of a kinematic hardening model, although the effect is minor in comparison to the overall magnitude of the cumulative strains. This trend is also observed in Scenario 7, but to a lesser extent due to the lower magnitude of δ .

Scenario 8 exhibits a measured peak field bending strain of 0.0171 mm/mm along Line A at the location of contact with the member on the left side, which is not seen on the right side of the measured results or in the FE predictions (Figure 11). This can be attributed to a combination of imperfections in the reaction frame and asymmetry in bolt tightening (Gerbo et al., 2018). As discussed in reference to Scenario 6, this shows that some asymmetry is to be expected during field bending which cannot be captured by a symmetric FE model.

For Scenario 1, along lines B and C, the numerical models tend to overpredict the measured

peak field bending strain at the member contact locations by approximately 10-15%. This is partially due to the strain measurement length used in the DIC calculations [the gauge length is 2.91 mm (0.114 in.) which is nearly double the mesh size in the FE models]. The resulting data av-387 eraging in DIC reduces the value of localized peaks. Another potential factor is the radius of the 388 fillet [1.27 mm (0.0500 in.)] used for all of the FE models. This value was selected based on 389 approximate fillet radius measurements of the fabricated frame which varies due to the irregular 390 nature of manually softening edges with an angle grinder. Further numerical modeling found that 391 a larger fillet radius in the member at the point of contact with the top plate will result in a reduced 392 peak strain [e.g., for a 3.81 mm (0.150 in.) radius, the predicted peak strain reduced by 24% on the 393 compressive face and by 3% on the tensile face]. Scenario 1 is particularly susceptible to the data 394 averaging and fillet radius issues because it has a high positive δ localizing strain at the member 395 contact location. 396

Overall, the prefabrication process dominates the cumulative strains in all scenarios (Figure 11). Any small differences between measured and predicted field bending strains discussed above are negligible compared to the cumulative strains. Both the measured and predicted cumulative strains are all very similar in the prebent region of the top plate. The predicted cumulative strains in the prebent regions of the bottom plates differ more from the measured results (i.e., 20% difference in the peak cumulative strain in Scenario 8) than the top plates (i.e., 5% difference in the peak cumulative strains in Scenario 8) due to the Bauschinger effect.

Summary 404

397

398

399

400

401

403

407

409

The developed FE modeling approach is able to predict circumferential surface strain distribu-405 tions and magnitudes in the plates from field bending and the cumulative fabrication process for a 406 wide variety of scenarios, including varying amount and direction of plate bend as well as varying plate angle (data for Scenarios 9-13 not shown for conciseness). Cumulative strains are dominated 408 by prefabrication and the numerical modeling approach is capable of accurately capturing these cumulative strains. The simplifying assumptions of symmetric bolt tightening and idealized ge-410 ometry of the reaction frame have negligible impact on the ability of the FE models to accurately capture plate behavior during field bending and the cumulative fabrication process. The isotropic material model, which does not account for the Bauschinger effect, resulted in small differences between the measured and predicted field bending strains. However, these are insignificant compared to the magnitude of the cumulative strains.

PARAMETRIC STUDY

With the numerical FE modeling approach validated, a parametric study was performed to 417 investigate the effect of (1) bolt diameter (d_b) , (2) plate thickness (t_s) , and (3) member thickness 418 (t_m) on residual bolt strains from field installation and on plate circumferential surface strains from 419 field bending and the cumulative fabrication process. The plate bend radii were varied to maintain 420 a constant ratio of radius to plate thickness ($r_b = r_t = 8t_s$). By maintaining the radius-to-plate-421 thickness ratio, the magnitude of the peak prefabrication strains in the plates is approximately the 422 same, though the width of the prebent section varies. A total of 11 scenarios were investigated 423 in comparison to a benchmark (Scenario A) with the same bolt diameter (d_b) , plate thickness (t_s) , 424 and member thickness (t_m) as studied in the experimental program. The plate angles $(\gamma = \beta =$ 10°), member angles ($\alpha = 12.5^{\circ}$), and relative ply angles ($\delta = 2.5^{\circ}$) were constant and the same as Scenario 6.

Effect of Bolt Diameter

Increasing the bolt diameter reduces bolt strains induced by field bending in most Scenarios, 429 as expected (Figure 12). In comparison to the experimental program (e.g., Figure 3), the peak 430 strains are concentrated in the reduced cross-section as opposed to the bolt shank for all parametric 431 results. This is because the experimentally tested bolts had longer shanks (to facilitate testing pro-432 tocol) which pushed the threaded region away from the shear plane. The parametric results have 433 more realistic bolt shank lengths (due to elimination of the spacers used to facilitate experimen-434 tal testing), such that the reduced cross-section, while still not in the shear plane, is much closer. 435 This concentrates bending strains, even from plate contact, in the reduced cross-section. Figure 13 436 shows the peak magnitude of curvature for the parametric scenarios, indicating curvature predom-437 inantly in the reduced cross-section.

Scenario G (most conservative) uses 25.4 mm (1.00 in.) diameter bolts to tighten 12.7 mm 439 (0.500 in.) thick plates, resulting in bolt strains below 0.0277 mm/mm. This is predominantly axial strain, as demonstrated by the low peak curvature [0.0226 deg/mm (0.574 deg/in.)]. Scenario C (least conservative) uses 19.2 mm (0.750 in.) diameter bolts to tighten 19.2 mm (0.750 in.) thick 442 plates, resulting in noticeable bending with peak tensile strains of 0.109 mm/mm, peak compressive 443 strains of 0.130 mm/mm, and peak curvature of 0.461 deg/mm (11.7 deg/in.) (Figure 12). In 444 general, the bending and therefore curvature increases with increasing bolt deformation (e_b) as 445 found in the experimental results (Figure 13). However, Scenario F, which has the same e_b value 446 as Scenario C, has lower peak curvature [0.354 deg/mm (8.99 deg/in.)] yet higher strains (0.133 447 mm/mm peak tensile strains and 0.195 mm/mm peak compressive strains). This is because the 448 the larger bolt diameter than Scenario C (17% difference) requires higher strain (22% higher peak 449 tensile strain and 50% higher peak compressive strain than Scenario C) to accommodate the same 450 high bolt deformation (e_b) . 451

Figure 14 shows that the bolt diameter is weakly inversely proportional to the induced field bending strains in the plates (focusing on strains away from the bolt hole locations), with larger bolts leading to slightly lower plate strains than smaller bolts. This is due to the larger area over which the clamping force is induced, leading to more evenly distributed strains during the field bending process. The cumulative strains for a given plate thickness are not significantly impacted by bolt diameter as they are dominated by the prefabrication strains.

58 Effect of Plate Thickness

452

453

454

455

457

For a given bolt diameter, an increase in plate thickness results in higher bolt strains (Figure 12) and higher bolt curvature (Figure 13). For a bolt diameter of 19.1 mm (0.750 in.) (Scenarios A, B and C), the peak induced tensile strain varies from 0.0510 mm/mm to 0.109 mm/mm for plate thicknesses of 12.7 mm (0.500 in.) to 19.1 mm (0.750 in.), respectively, and the peak curvature increases from 0.241 deg/mm (6.12 deg/in.) to 0.461 deg/mm (11.7 deg/in.). This is partly due to the additional bolt force required to close connections with thicker plates, resulting in a higher moment from eccentric bolt head and nut contact. The bolt bending is also increased by thicker

plates because the eccentricity between the plate holes (e_h) increases, which results in larger required bolt deformation (e_b) . The bolt deformation is found to be positively correlated with the peak bolt strain (Figure 12) and peak curvature (Figure 13). It is therefore recommended that the bolt deformation (e_b) be below 3.18 mm (0.125 in.) to minimize bolt bending.

The relationship between plate thickness and peak bolt strain is most significant in the smallest 470 bolts [d_b = 19.1 mm (0.75 in.), Scenarios A, B and C], and least significant in the largest bolts [d_b = 471 25.4 mm (1.00 in.), Scenarios G, H and I] (Figure 12). This is likely due to the larger bolts having 472 a higher yield force, and therefore lower degrees of plastic behavior compared to the smaller bolts. 473 Recall that only plastic residual strains are reported. When considering the difference between 474 the thinnest and thickest plates, the peak tensile strain increases from 0.0277 mm/mm to 0.0316 475 mm/mm for the largest diameter bolts (i.e., Scenarios G - I), and from 0.0510 mm/mm to 0.109 476 mm/mm for the smallest diameter bolts (Scenarios A - C) (Figure 12). In order to keep the bolt 477 from experiencing significant increases in strain, it is recommended to use bolts with a diameter at 478 least 20% greater than the plate thickness (e.g., Scenario B). 479

The predicted peak field bending strains in the plates at the member contact locations are not significantly affected by the plate thickness (Figure 14). The cumulative plate strains are dominated by the prefabrication process, discussed in Gerbo et al. (2016), with field bending strains being an order of magnitude lower.

Effect of Member Thickness

Member thicknesses were varied to explore the plate and bolt behavior with more flexible members, corresponding to W10x88, W10x68 and W10x49 sections (Table 2). Connections with thicker members (i.e., Scenario A) are found to induce higher bolt bending strains (Figure 15) and curvature (Figure 13) than thinner members (i.e., Scenario K). This is because thicker members result in higher required bolt deformation (e_b).

A flexible (i.e., thin) member flange deforms more during field bending and therefore can reduce the peak field bending strains in the plates at the member contact locations along lines B and C. It is found that a thinner member flange results in lower induced plate strains during field

bending as expected. This difference is most significant between the thickest member flanges [t_m] = 25.1 mm (0.990 in.), Scenario A] and the thinnest member flanges [t_m] = 14.2 mm (0.560 in.), Scenario K], with a 26.2% reduction in peak field bending strain in the top plates, and a 12.2% reduction in the bottom plates. The cumulative strains are nearly indistinguishable between these three scenarios, as the minor differences in the field bending strains are overshadowed by the prefabrication strains.

499 Local Plate Strains

Local strain concentrations occur in the plates near the bolt holes [i.e., $x = \pm 150$ mm (5.91 in.) 500 on lines B and C in Figure 14] and are positively correlated with the bolt deformation (e_b) . These 50 strain concentrations can somewhat be seen in the measured results near this region in Figure 11. However, the measured strains are lower in magnitude than the FE predictions partially due to the 503 DIC view being blocked by the washers and bolt assembly, as well as the edge effect observed in DIC measurements as discussed in Gerbo et al. (2016). The FE models are therefore useful tools to be able to determine the peak strains near the bolt hole, not only on the plate surface but 506 also through the thickness of the plate. Increasing e_b results in increased local strains near the 507 plate holes due to the additional contact pressure between the bolt and the plate hole (Figure 16). 508 To keep local strains in the plates below the recommended 0.100 mm/mm [strains beyond 0.100 509 mm/mm have been found to result in reductions to ductility and fracture toughness (Keating and 510 Christian, 2012)], e_b should be kept below 3.18 mm (0.125 in.). 511

512 CONCLUSIONS

This paper presented an experimental investigation of bolt behavior in adjustable bolted steel plate connections during field installation, a validated numerical modeling approach, and a numerical parametric investigation of the impact of (1) bolt diameter, (2) plate thickness, and (3) member flange thickness on the strains induced in both the plates and bolts during field installation. Based on these experimental and numerical studies, the following conclusions are made. Note that these conclusions may only be relevant to the specific scenarios studied in this research.

• A bolt tightening procedure using 1 turn increments and a criss-cross pattern is recommended to ensure evenly distributed strains in the four bolts of the connection, consistent with the recommendations in Gerbo et al. (2018) for evenly distributed plate strains. Tightening procedures with 3 or more turns per increment were found to result in gouging to the surface of the bolt, and significant asymmetries in strains among the four bolts of the connection. By using 1 turn increments, the bolts are evenly tightened, resulting in more uniform behavior across the connection.

- Prefabrication strains (approximately 0.06 mm/mm) dominate behavior of the plates compared to field bending strains (approximately 0.006 mm/mm) by an order of magnitude.
 Recommendations regarding the strains induced during prefabrication are discussed in Gerbo et al. (2016). The parameters chosen for prefabrication (i.e., bend radius and plate thickness) play a more significant role in determining cumulative strains than the parameters chosen during field bending.
- The bolt deformation (e_b) should not exceed 3.18 mm (0.125 in.) to reduce bolt bending strains and to reduce local strain concentrations in the plates near the bolt holes. Considering the formulation for e_b and the shallow member angles (α) investigated in this research, the most effective means of reducing e_b is to reduce the bolt diameter (d_b) or increase the plate hole diameter (d_{ph}) , with reduced benefit from decreasing the member thickness (t_m) or the plate thickness (t_s) . Reducing the bolt diameter (d_b) could have a negative impact on connection performance, which will be an area of future research. Increasing the plate hole diameter (d_{ph}) , beyond the currently investigated oversized holes, may also negatively impact connection performance and potentially also durability.
- To ensure adequate bolt strength to close a given connection, it is recommended to use bolt diameters (d_b) at least 20% larger than the plate thickness (t_s) . However, increased bolt diameter can have a negative impact on connections with high e_b values, as it can increase the bolt bending strains. Bolt diameter is weakly inversely proportional to the magnitude of the induced field bending strains in the plates.

• Thinner member flanges can lower the strains induced in the plates during field bending by up to approximately 26%. More flexible members [i.e., $t_m \le 19.6 \text{ mm } (0.770 \text{ in.})$] conform more to the plates' initial shape, while inducing negligible strains in the member. Member thickness (t_m) does not play a direct role in the induced strain in the bolts. However, it is used in the calculation of e_b , and therefore can indirectly affect bolt bending.

The adjustable bolted steel plate connection shows promise to provide adjustability in steel plate connections, and to accommodate significant construction and manufacturing tolerances. Future work includes evaluation of connection performance under service and ultimate limit states. Importantly, the research findings provide useful limits on bolt tightening procedures, bolt deformation (e_b) , and relative sizes of bolts and plates for any misaligned (non-flush) bolted splice connections. This enables force fitting to be performed in a controlled manner in which the strains induced in the bolts and plates during bolt tightening are well understood. The future research in understanding the connection performance under service and ultimate limit states will provide further guidance on these procedures.

60 ACKNOWLEDGMENTS

This material is based upon work supported by the National Science Foundation under Grant
No. CMMI-1351272. The support of Program Managers Drs. Kishor Mehta and Y. Grace Hsuan
is gratefully acknowledged.

564 REFERENCES

- 565 AASHTO (2014). AASHTO LRFD Bridge Design Specifications, Customary U.S. Units. American
- Association of State Highway and Transportation Officials (AASHTO), 7th Edition, with 2015
- and 2016 Interim Revisions, Washington, D.C.
- ABAQUS (2014). "ABAQUS/Standard Analysis User's Manual Version 6.14. Dassault Systemes,
- Waltham, MA.
- ASTM (2014a). "ASTM A325-14: Standard specification for structural bolts, steel, heat treated,
- 120/105 ksi minimum tensile strength." ASTM International. West Conshohocken, PA.
- 572 ASTM (2014b). "ASTM A36/A36M-14: Standard specification for carbon structural steel."
- ASTM International. West Conshohocken, PA.
- ASTM (2015). "ASTM A992-15: Standard specification for structural steel shapes." ASTM Inter-
- 575 national.
- 576 ASTM (2018). "ASTM F436/F436M-18a: Standard specification for hardened steel washers inch
- and metric dimensions." ASTM International. West Conshohocken, PA.
- ⁵⁷⁸ Chesson, E. and Munse, W. H. (1965). "Studies of the behavior of high strength bolts and bolted
- joints." Engineering Experiment Station, University of Illinois, 469.
- Douty, R. T. and McGuire, W. (1965). "High strength bolted moment connections." Journal of the
- 581 Structural Division, American Society of Civil Engineers, 91(ST2), 101–128.
- Ferro (2016). "CerMark laser marking materials. http://www.ferro.com/Our +
- Products/ColorsGlass/FunctionalIndustrial/CerMark/ (January 26, 2016).
- Gerbo, E. J., Thrall, A. P., Smith, B. J., and Zoli, T. P. (2016). "Full-field measurement of residual
- strains in cold bent steel plates." *Journal of Constructional Steel Research*, 127, 187–203.

- Gerbo, E. J., Wang, Y., Tumbeva, M. D., Thrall, A. P., Smith, B. J., and Zoli, T. P. (2018). "Behavior
- of an adjustable bolted steel plate connection during field installation." Journal of Structural
- Engineering, 144(3), 04017223.
- Gerbo, E. J., Wang, Y., Tumbeva, M. D., Thrall, A. P., Smith, B. J., and Zoli, T. P. (2019). "Closure
- to 'Behavior of an Adjustable Bolted Steel Plate Connection during Field Installation' by Evan
- J. Gerbo, Yao Wang, Mirela D. Tumbeva, Ashley P. Thrall, Brian J. Smith, and Theodore P.
- Zoli." *Journal of Structural Engineering*, 145(3), 07018015.
- Keating, P. B. and Christian, L. C. (2012). "Effects of bending and heat on the ductility and fracture
- toughness of flange plate. Technical Report No. FHWA/TX-10/0-4624-2.
- 595 Kulak, G. L., Fisher, J. W., and Struik, J. H. A. (2001). Guide to Design Criteria for Bolted and
- 8596 Riveted Joints. American Institute of Steel Construction, 2nd Edition, Chicago, I.L.
- Munse, W. H., Peterson, K. S., and Shesson, E. (1959). "Strength of rivets and bolts in tension."
- Journal of the Structural Division, American Society of Civil Engineers, 85(ST3), 7–28.
- Rajasekharan, N. S., Birkemoe, P. C., and Munse, W. H. (1974). "High strength bolts subject to
- tension and prying." Journal of the Structural Division, American Society of Civil Engineers,
- 601 100, 351–372.
- Research Council on Structural Connections (2014). "Specifications for Structural Joints Using
- 603 High-Strength Bolts.

604 List of Tables

605	1	Experimentally tested connection parameters. * Abbreviations for bolt tightening	
606		procedure, with indications for bolt number: $(x) = criss-cross (1-2-3-4), (cw) =$	
607		clockwise (1-4-2-3), (ccw) = counter-clockwise (4-1-3-2) (Figure 1)	26
608	2	Parametric study connection parameters. Bolded scenario indicates benchmark	
609		case. Initial plate angles ($\gamma = \beta = 10^{\circ}$), member angles ($\alpha = 12.5^{\circ}$), and relative	
610		ply angles ($\delta = 2.5^{\circ}$) are constant	27

TABLE 1. Experimentally tested connection parameters. * Abbreviations for bolt tightening procedure, with indications for bolt number: (x) = criss-cross (1-2-3-4), (cw) = clockwise (1-4-2-3), (ccw) = counter-clockwise (4-1-3-2) (Figure 1).

Scenario	21 - B	0.	δ	1 _1	Tightoning Procedure	
Scenario	$\gamma = \beta$	α		$l_1=l_2$	Tightening Procedure	e_b
	(deg.)	(deg.)	(deg.)	(mm)	Increment (Pattern*)	(mm)
1	10	17.5	7.5	483	1 turn/bolt (x)	9.65
2	10	17.5	7.5	483	3 turns/bolt (x)	9.65
3	10	17.5	7.5	483	Fully tighten bolt (x)	9.65
4	10	17.5	7.5	483	1 turn/bolt (cw)	9.65
5	10	17.5	7.5	483	1 turn/bolt (ccw)	9.65
6	10	12.5	2.5	483	1 turn/bolt (x)	4.29
7	10	7.5	-2.5	483	1 turn/bolt (x)	-0.377
8	10	2.5	-7.5	483	1 turn/bolt (x)	-4.25
9	0	2.5	2.5	381	1 turn/bolt (x)	-3.04
10	5	2.5	-2.5	432	1 turn/bolt (x)	-3.28
11	5	7.5	2.5	432	1 turn/bolt (x)	0.585
12	15	12.5	-2.5	533	1 turn/bolt (x)	2.36
13	15	17.5	2.5	533	1 turn/bolt (x)	8.15
14	0	0	0	381	1 turn/bolt (x)	-4.76

Source: Reprinted from Gerbo et al. (2018), ©ASCE.

TABLE 2. Parametric study connection parameters. Bolded scenario indicates benchmark case. Initial plate angles ($\gamma = \beta = 10^{\circ}$), member angles ($\alpha = 12.5^{\circ}$), and relative ply angles ($\delta = 2.5^{\circ}$) are constant.

	d_b	t_s	t_m	$l_1 = l_2$	e_b
Scenario	(mm)	(mm)	(mm)	(mm)	(mm)
A	19.1	12.7	25.1	9.50	4.29
В	19.1	15.9	25.1	9.50	5.00
С	19.1	19.1	25.1	9.50	5.70
D	22.2	12.7	25.1	9.50	4.29
Е	22.2	15.9	25.1	9.50	5.00
F	22.2	19.1	25.1	9.50	5.70
G	25.4	12.7	25.1	12.7	2.70
Н	25.4	15.9	25.1	12.7	3.41
I	25.4	19.1	25.1	12.7	4.11
J	19.1	12.7	19.6	12.7	3.05
K	19.1	12.7	14.2	12.7	1.87

611 List of Figures

612	1	Adjustable bolted steel plate connection: (A) elevation view of initial un-tightened	
613		connection; (B) elevation view of final tightened connection (adapted from Gerbo	
614		et al. 2019); (C) 3D view of the final tightened connection; (D) plan view of fi-	
615		nal tightened connection; (E) experimental test setup; (F) bolt-tightening tools	
616		(reprinted from Gerbo et al. 2018, ©ASCE.)	30
617	2	Geometric parameters: (A) untightened state (exaggerated); (B) flat plates; (C) bolt	
618		eccentricity; (D) example deformation of scenario with positive δ ; (E) example	
619		deformation of scenario with negative δ . [Adapted (a and b) from Gerbo et al.	
620		2018, ©ASCE.]	31
621	3	Scenario 1: Longitudinal bolt surface strains (ϵ_y)	32
622	4	FE model showing (A) boundary conditions for symmetry; (B) boundary condi-	
623		tions for rigid member.	33
624	5	Effect of bolt-tightening procedure: Measured and predicted curvature (ϕ) along	
625		bolt axis for Scenarios 1, 2, 4, and 5	34
626	6	Effect of amount and direction of plate bending: Measured and predicted curvature	
627		(ϕ) along bolt axis for Scenarios 1, 6, 7 and 8	35
628	7	FE predictions of maximum magnitude of curvature (ϕ) for experimentally tested	
629		scenarios	36
630	8	Effect of plate angle: Measured and predicted curvature (ϕ) along bolt axis Sce-	
631		narios 9, 10, 11, 12 and 13	37
632	9	Longitudinal lines for data identification. Numbers indicate bolt identification.	
633		(Reprinted from Gerbo et al. 2018, ©ASCE.)	38
634	10	Scenario 6: Circumferential plate surface strains (ϵ_x) . (Data from Gerbo et al.	
635		2018, ©ASCE.)	39

636	11	Varying amount and direction of bend: measured DIC circumferential surface	
637		strain (ϵ_x) and FE predictions along lines A-D (Figure 9) for Scenarios 1, 6, 7,	
638		and 8 (Table 1). (Data from Gerbo et al. 2018, ©ASCE.)	40
639	12	Effect of plate thickness and bolt diameter: Predicted longitudinal bolt surface	
640		strains (ϵ_y) . Letters indicate Scenario	41
641	13	FE predictions of maximum magnitude of curvature (ϕ) for parametric scenarios	42
642	14	Effect of varying bolt diameter (d_b) and plate thickness (t_s) : Predicted plate field	
643		bending and cumulative circumferential surface strains (ϵ_x) for Scenarios A-I (Ta-	
644		ble 2)	43
645	15	Effect of varying member flange thickness (t_m) : Predicted longitudinal bolt surface	
646		strains (ϵ_y). Letters indicate Scenario	44
647	16	Predicted local peak circumferential strain (ϵ_x) in the plates near the bolt holes	
648		with varying bolt deformation (e_i)	45

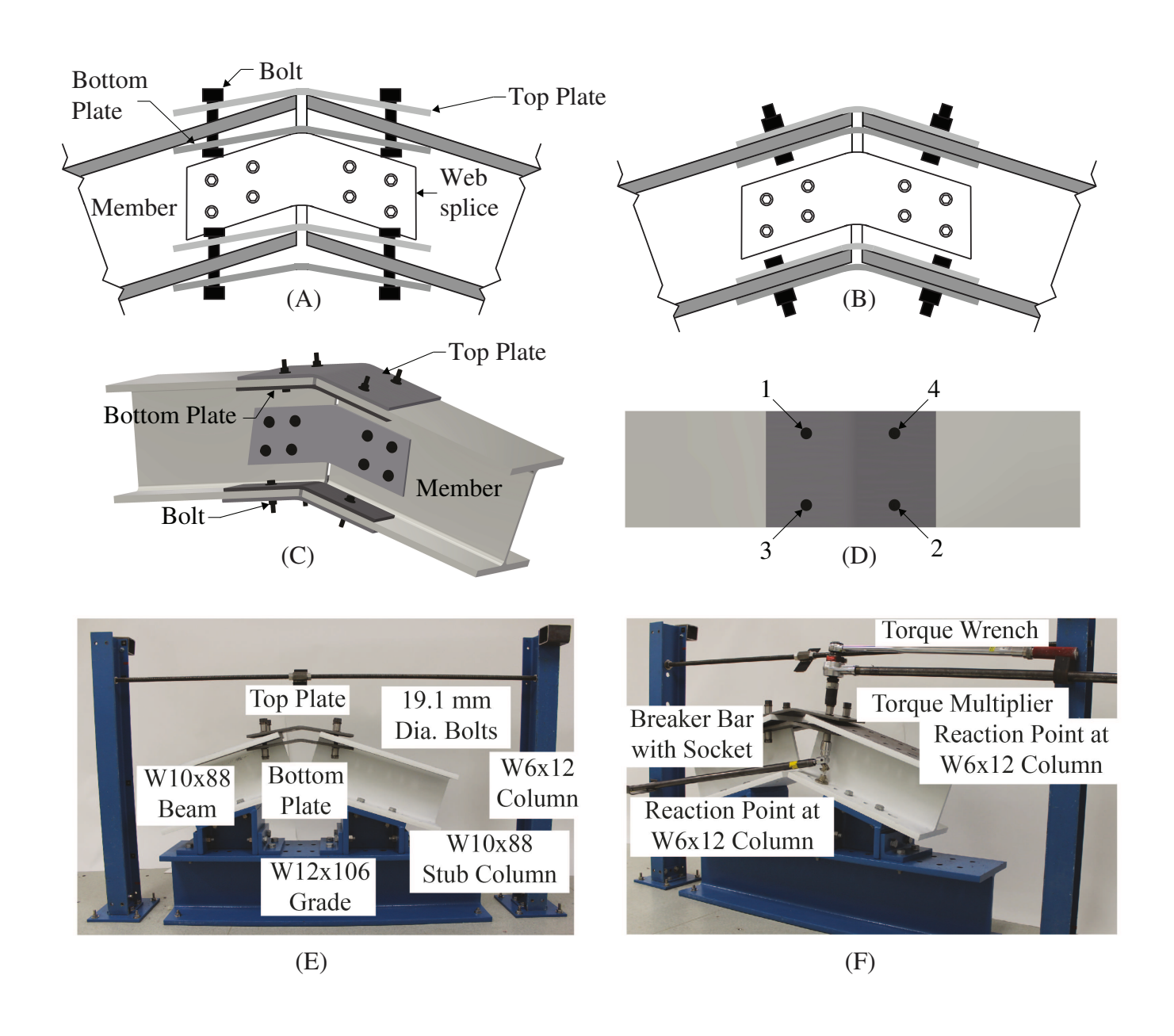


FIG. 1. Adjustable bolted steel plate connection: (A) elevation view of initial untightened connection; (B) elevation view of final tightened connection (adapted from Gerbo et al. 2019); (C) 3D view of the final tightened connection; (D) plan view of final tightened connection; (E) experimental test setup; (F) bolt-tightening tools (reprinted from Gerbo et al. 2018, ©ASCE.)

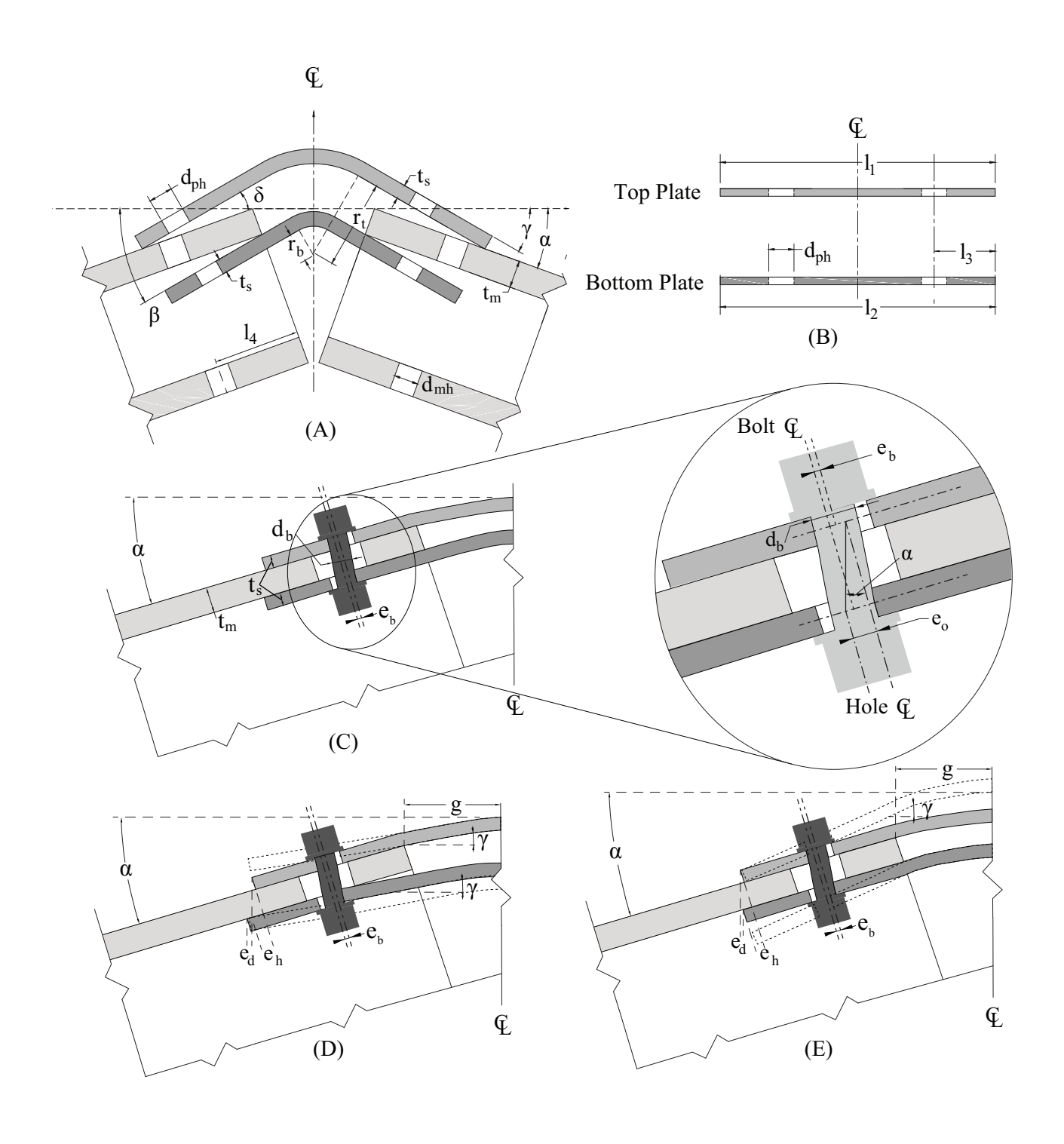


FIG. 2. Geometric parameters: (A) untightened state (exaggerated); (B) flat plates; (C) bolt eccentricity; (D) example deformation of scenario with positive δ ; (E) example deformation of scenario with negative δ . [Adapted (a and b) from Gerbo et al. 2018, ©ASCE.]

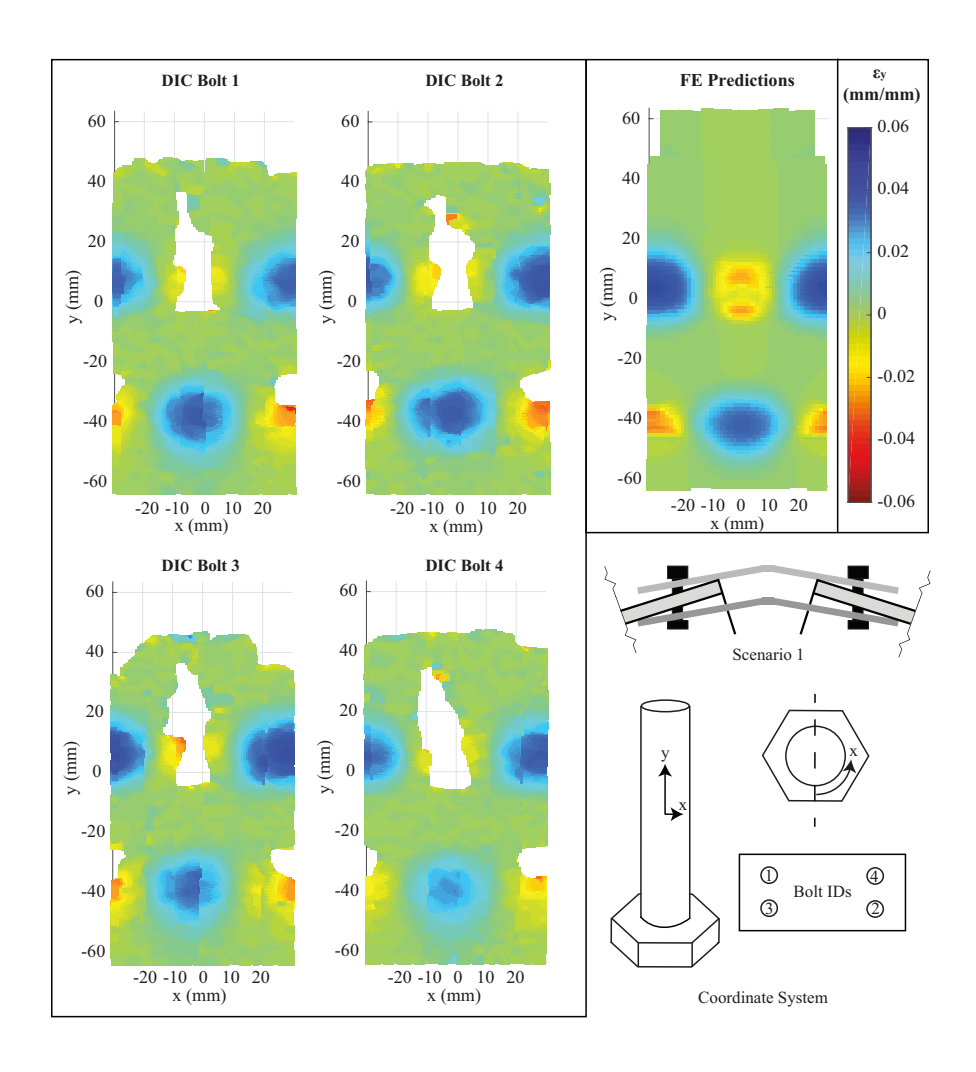


FIG. 3. Scenario 1: Longitudinal bolt surface strains (ϵ_y).

32

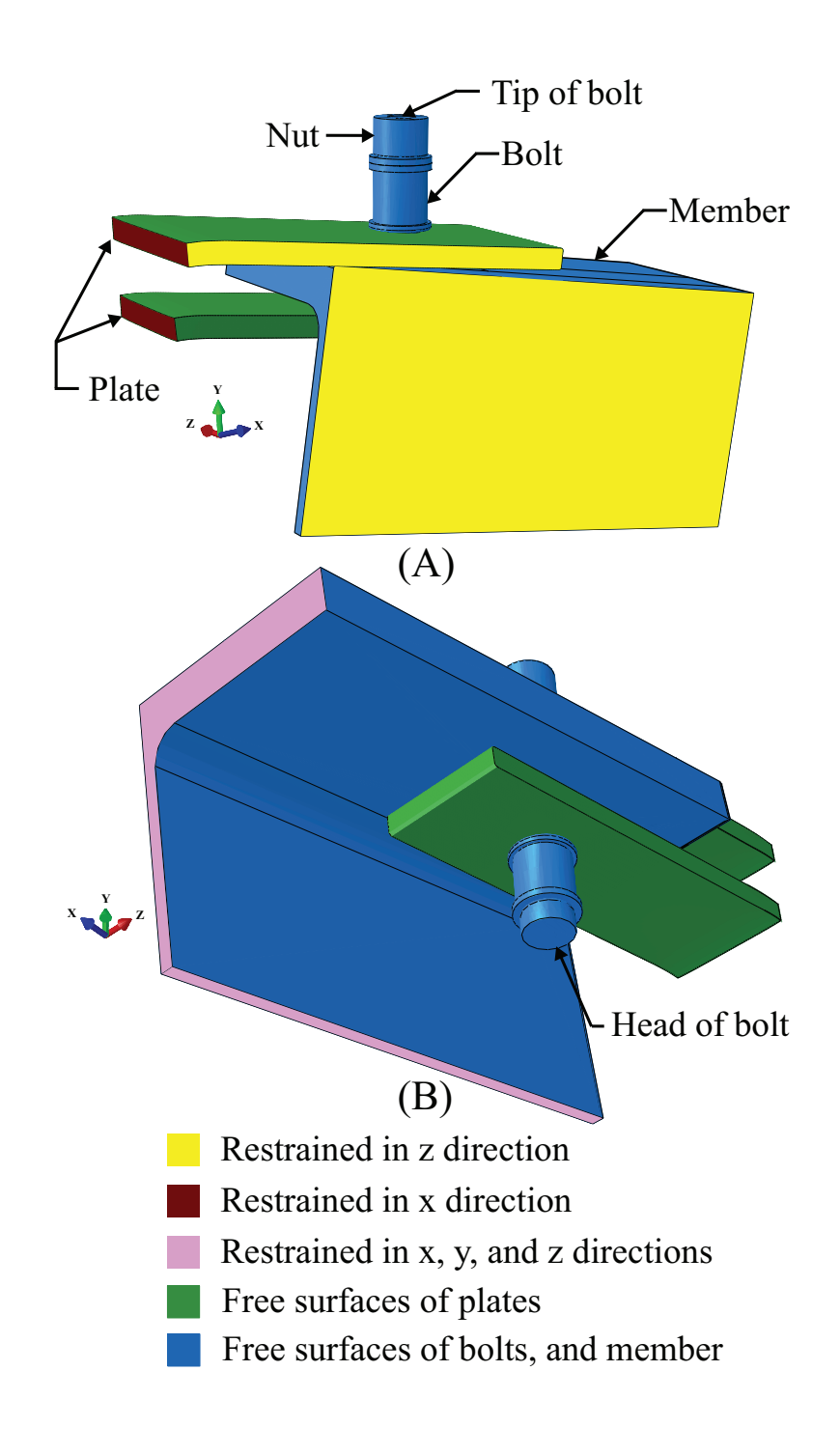


FIG. 4. FE model showing (A) boundary conditions for symmetry; (B) boundary conditions for rigid member.

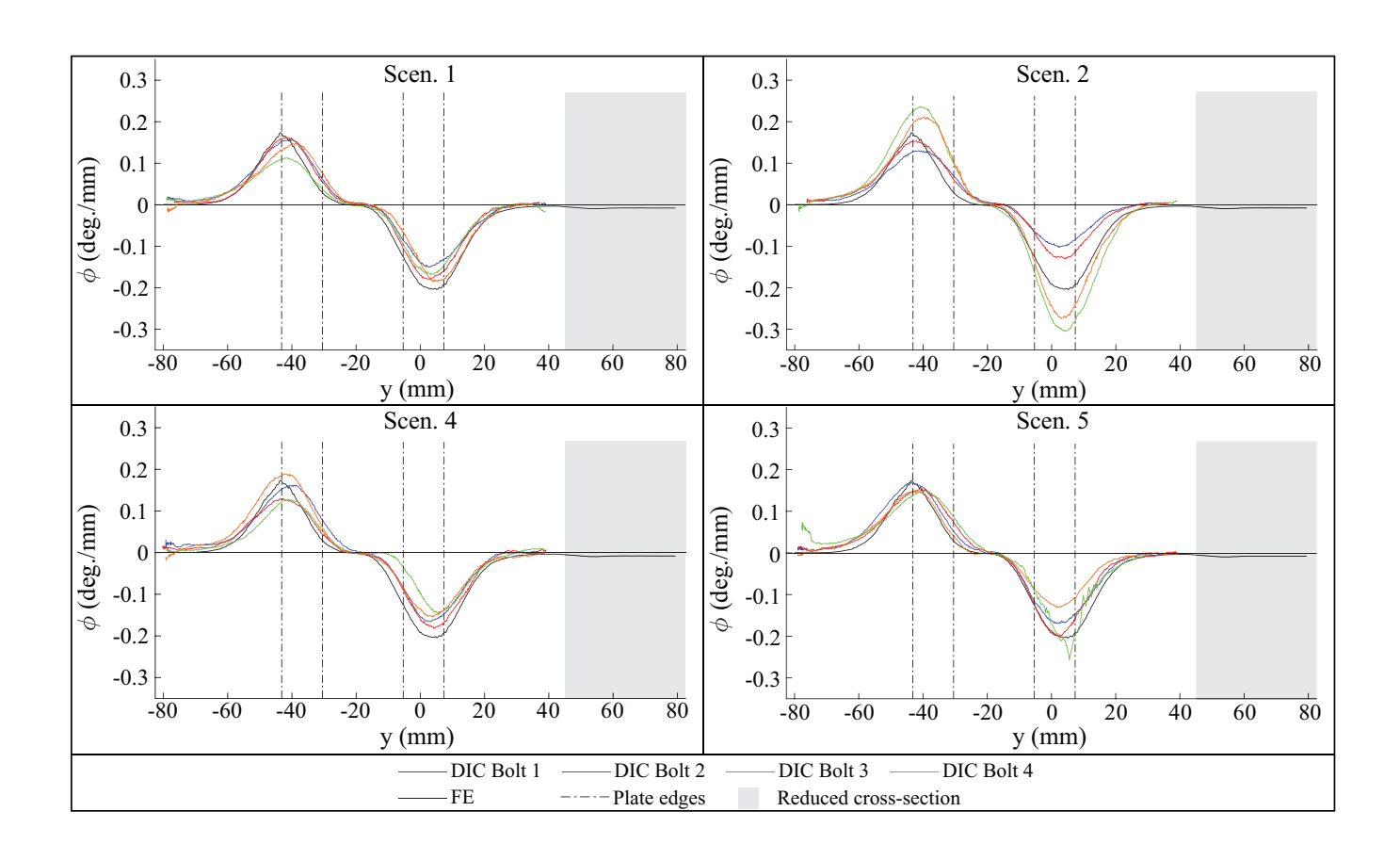


FIG. 5. Effect of bolt-tightening procedure: Measured and predicted curvature (ϕ) along bolt axis for Scenarios 1, 2, 4, and 5.

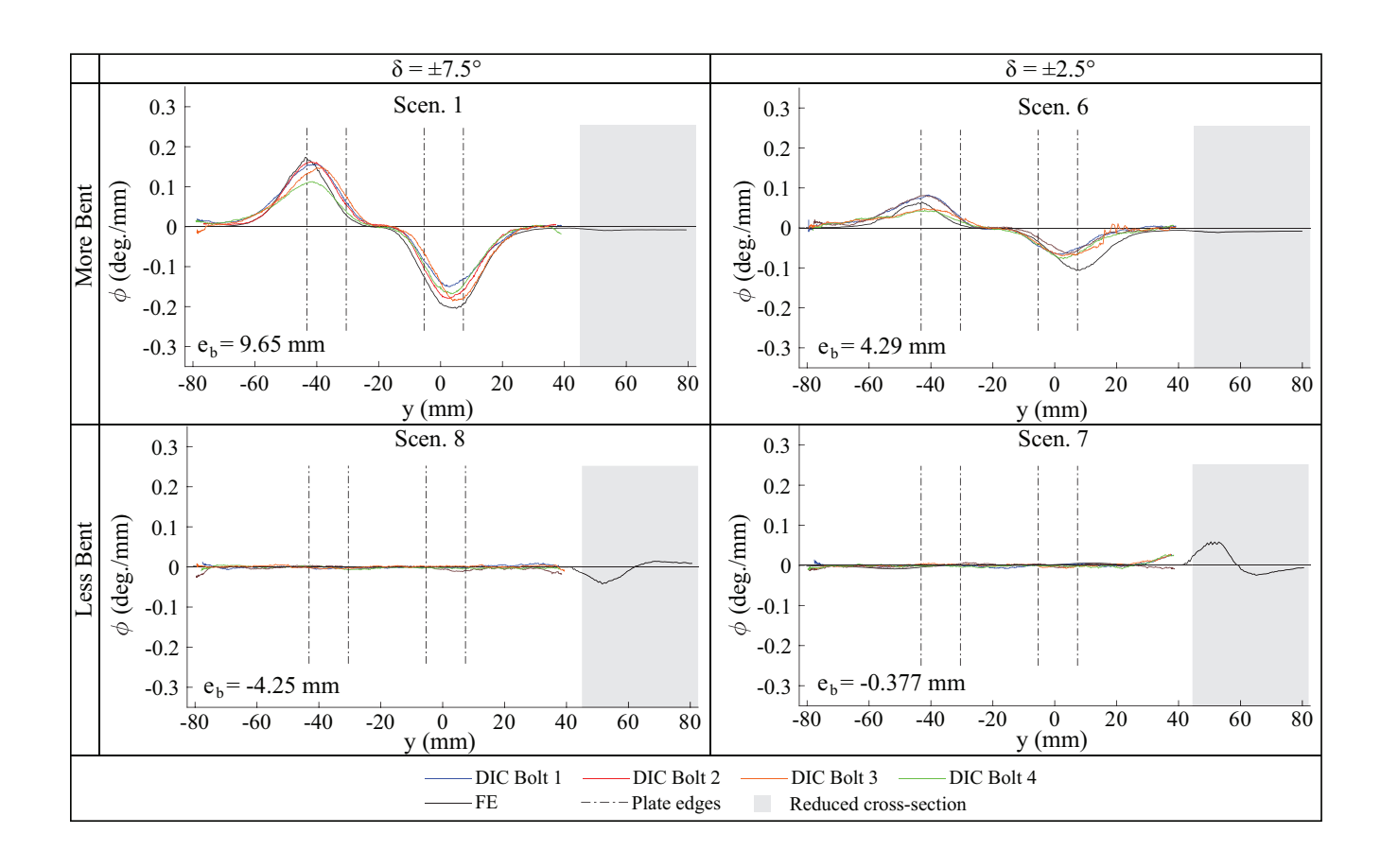


FIG. 6. Effect of amount and direction of plate bending: Measured and predicted curvature (ϕ) along bolt axis for Scenarios 1, 6, 7 and 8.

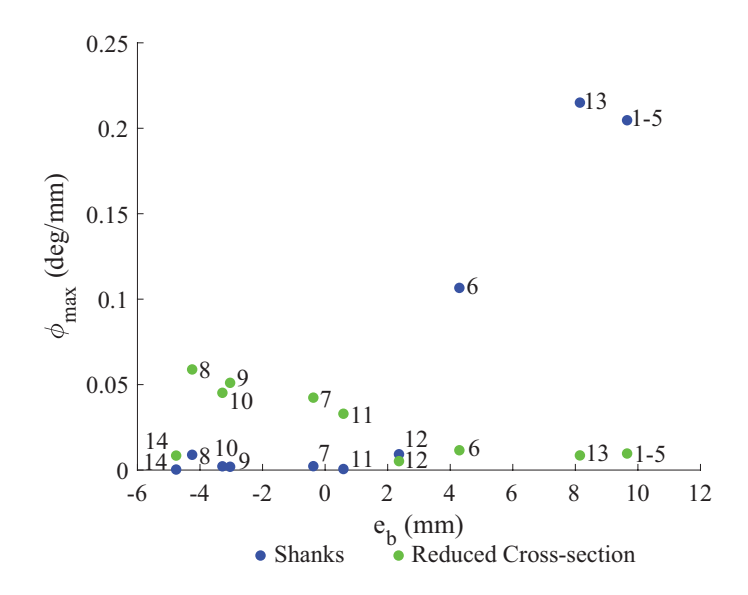


FIG. 7. FE predictions of maximum magnitude of curvature (ϕ) for experimentally tested scenarios.

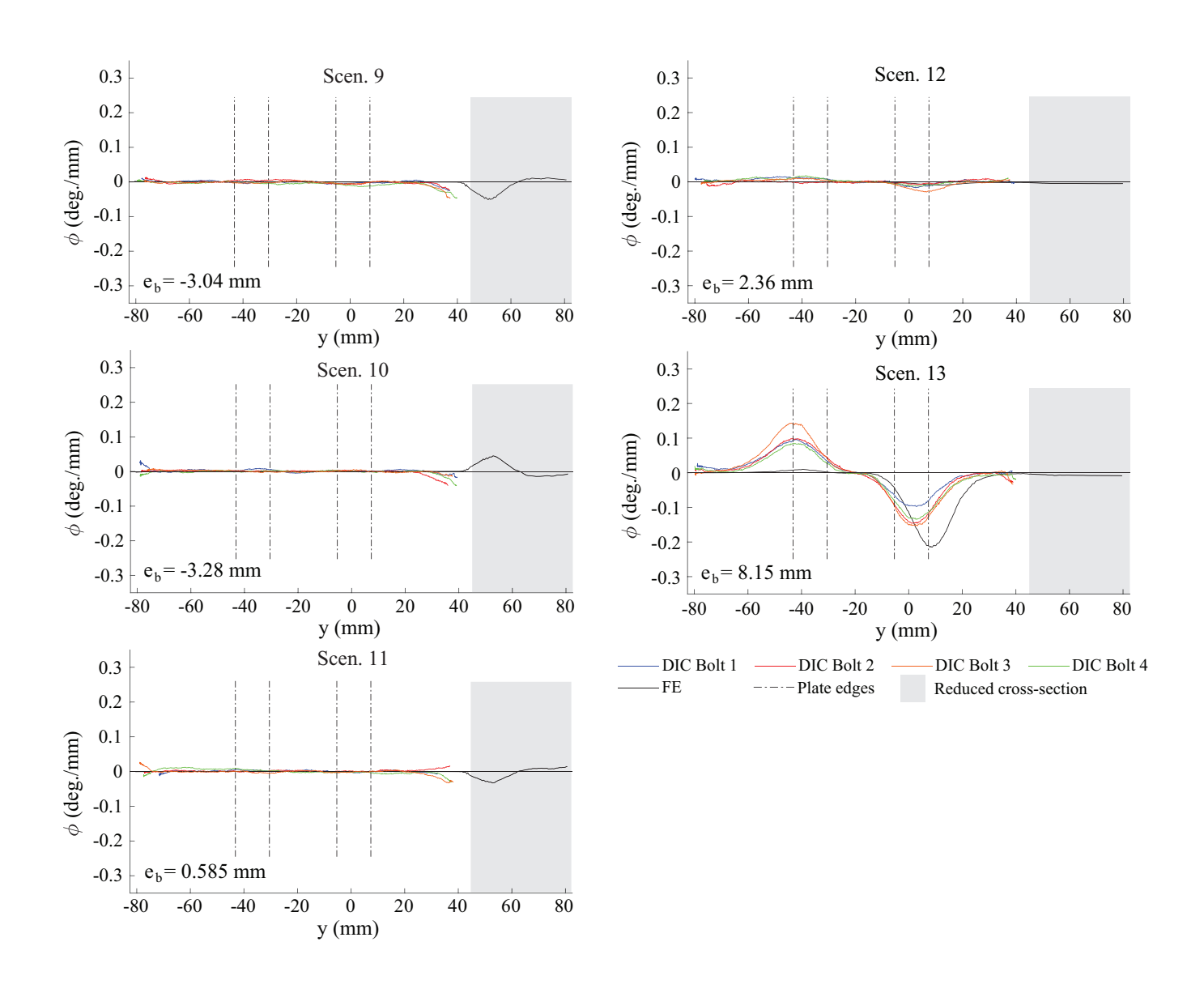


FIG. 8. Effect of plate angle: Measured and predicted curvature (ϕ) along bolt axis Scenarios 9, 10, 11, 12 and 13.

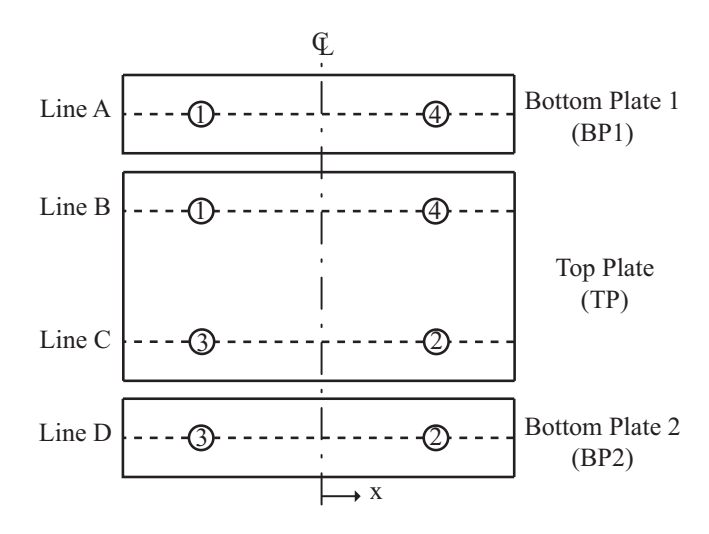


FIG. 9. Longitudinal lines for data identification. Numbers indicate bolt identification. (Reprinted from Gerbo et al. 2018, \bigcirc ASCE.)

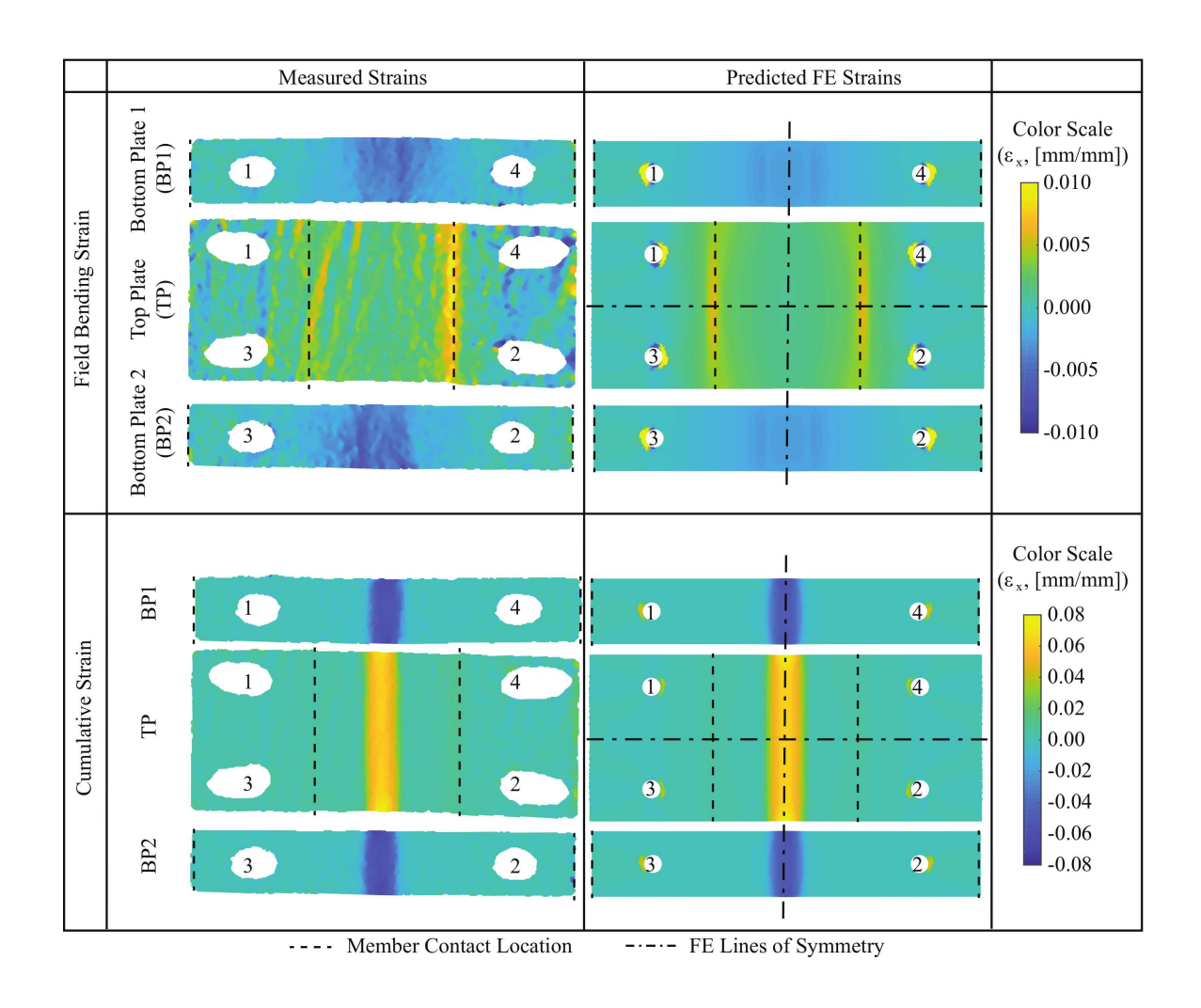


FIG. 10. Scenario 6: Circumferential plate surface strains (ϵ_x). (Data from Gerbo et al. 2018, ©ASCE.)

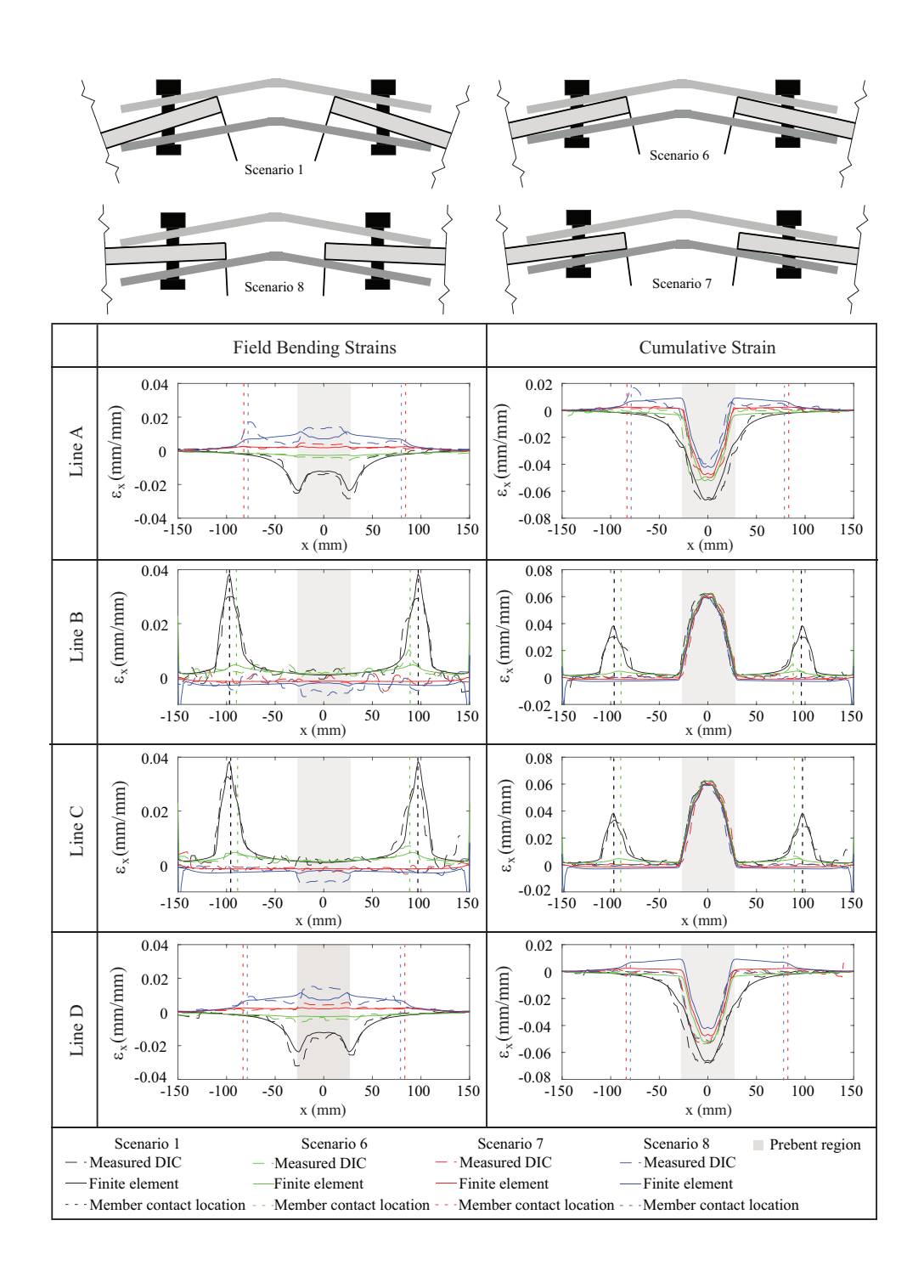


FIG. 11. Varying amount and direction of bend: measured DIC circumferential surface strain (ϵ_x) and FE predictions along lines A-D (Figure 9) for Scenarios 1, 6, 7, and 8 (Table 1). (Data from Gerbo et al. 2018, ©ASCE.)

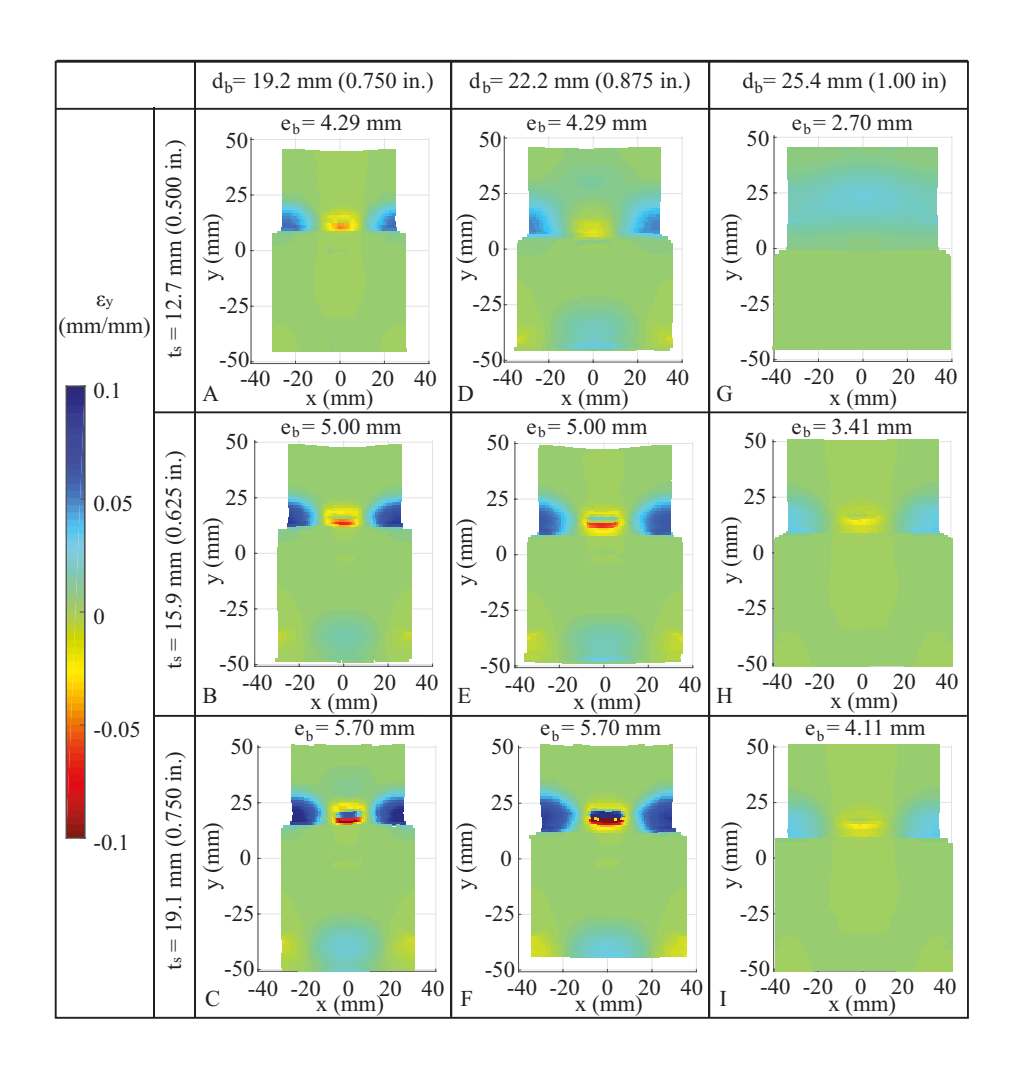


FIG. 12. Effect of plate thickness and bolt diameter: Predicted longitudinal bolt surface strains (ϵ_y). Letters indicate Scenario.

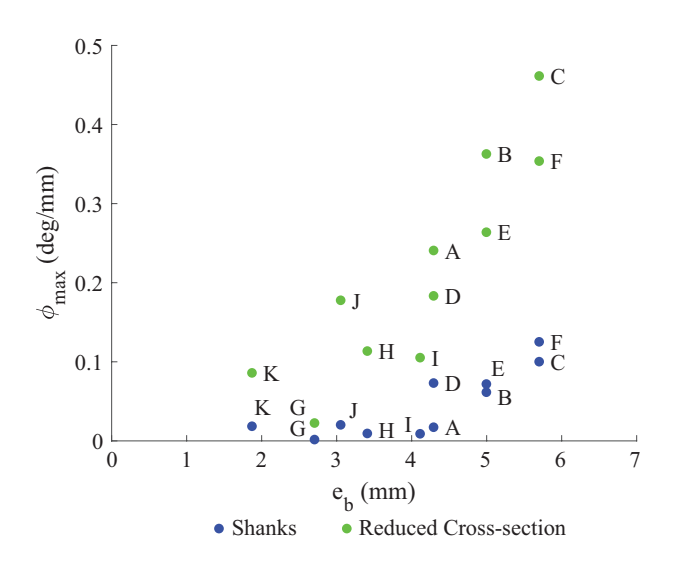


FIG. 13. FE predictions of maximum magnitude of curvature (ϕ) for parametric scenarios.

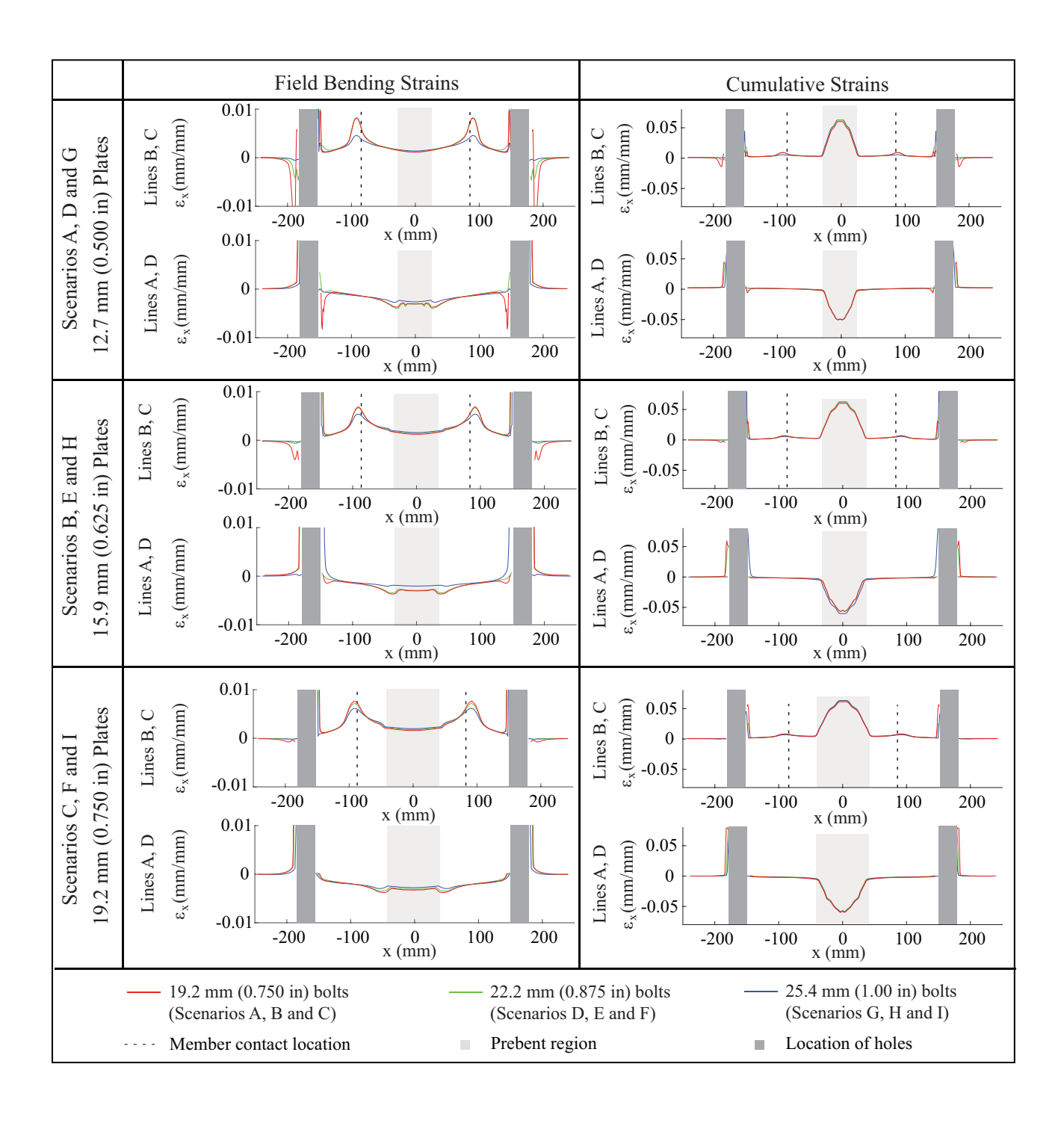


FIG. 14. Effect of varying bolt diameter (d_b) and plate thickness (t_s): Predicted plate field bending and cumulative circumferential surface strains (ϵ_x) for Scenarios A-I (Table 2).

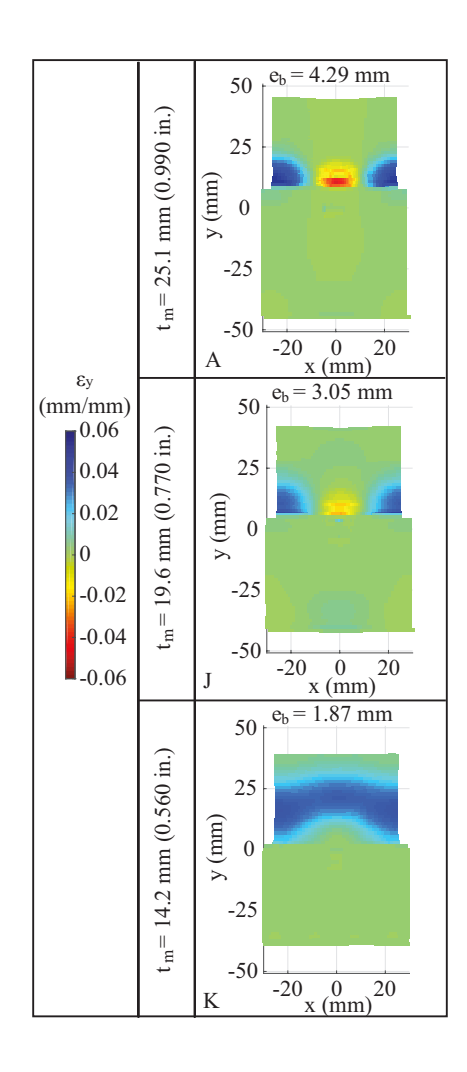


FIG. 15. Effect of varying member flange thickness (t_m): Predicted longitudinal bolt surface strains (ϵ_y). Letters indicate Scenario.

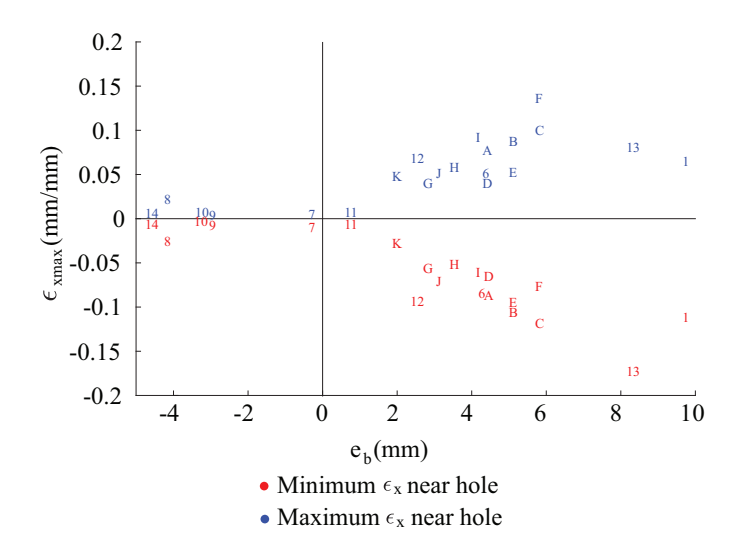


FIG. 16. Predicted local peak circumferential strain (ϵ_x) in the plates near the bolt holes with varying bolt deformation (e_b).